Neuromorphic
Computing and
Engineering

PAPER • OPEN ACCESS

Neuromorphic place cells

To cite this article: Zhaoqi Chen *et al* 2024 *Neuromorph. Comput. Eng.* **4** 024009

NEUROMORPHIC
Computing and Engineering

CrossMark

OPEN ACCESS

RECEIVED
7 February 2024

REVISED
28 April 2024

ACCEPTED FOR PUBLICATION
8 May 2024

PUBLISHED
20 May 2024

PAPER

Neuromorphic place cells

Zhaoqi Chen[*], **Alia Nasrallah and Ralph Etienne-Cummings**

The Johns Hopkins University, Baltimore, MD, United States of America

[*] Author to whom any correspondence should be addressed.

E-mail: zchen70@jhu.edu

Keywords: oscillatory interference, place cells, SLAM, neuromorphic engineering, hardware implementation

Abstract

A neuromorphic simultaneous localization and mapping (SLAM) system shows potential for more efficient implementation than its traditional counterpart. At the mean time a neuromorphic model of spatial encoding neurons in silicon could provide insights on the functionality and dynamic between each group of cells. Especially when realistic factors including variations and imperfections on the neural movement encoding are presented to challenge the existing hypothetical models for localization. We demonstrate a mixed-mode implementation for spatial encoding neurons including theta cells, egocentric place cells, and the typical allocentric place cells. Together, they form a biologically plausible network that could reproduce the localization functionality of place cells observed in rodents. The system consists of a theta chip with 128 theta cell units and an FPGA implementing 4 networks for egocentric place cells formation that provides the capability for tracking on a 11 by 11 place cell grid. Experimental results validate the robustness of our model when suffering from as much as 18% deviation, induced by parameter variations in analog circuits, from the mathematical model of theta cells. We provide a model for implementing dynamic neuromorphic SLAM systems for dynamic-scale mapping of cluttered environments, even when subject to significant errors in sensory measurements and real-time analog computation. We also suggest a robust approach for the network topology of spatial cells that can mitigate neural non-uniformity and provides a hypothesis for the function of grid cells and the existence of egocentric place cells.

1. Introduction

Navigation and localization are essential capabilities for animals and humans to survive in complex terrains. As they depart from their homes, they can plan a path through obstacles while advancing towards their targets and remember the path to return home. Interestingly, when exploring a new environment, animals can form a concept of the environment that couples spatial location with sensory stimuli to remember locations of, for example, food and danger. This behavior coincides with the scenario of autonomous robots navigating without a pre-charted map. In the robotics community, this problem is called simultaneous localization and mapping [1] (SLAM) and is conceptualized as the computational problem of creating a map of an initially unknown environment and localizing the robot while exploring. However, typical SLAM algorithms require complex computations to handle a large number of sensory inputs and internal memory, resulting in high computational and energy demands. Animals, in contrast, achieve SLAM without explicit mathematical computations and can even navigate in darkness with relatively few sensory inputs. Many researchers [2–6] propose that the neuroscience study of how animal brains navigate and localize would help in developing more energy- and computation-efficient SLAM algorithms.

The memorizing of environmental information with location implies some form of spatial encoding within the brain. Neuroscience has already observed several classes of neurons whose firing behaviors couple with the animal's spatial location. In particular, 'place cells' was discovered in the rat hippocampus with their firing rate is high only when the animal is within a particular spatial location, which defines the associated place field [7]. Later, 'grid cells' that activate with spatial periodicity as the animal explores a given space was also observed [8]. When encountering an unfamiliar environment, new spatially specific behaviors such as relocation of firing fields of place cells, and change in periodicities of grid cells are generated and persist until further changes of the environment [9–11], demonstrating their mapping capabilities and role in navigation.

Such discoveries have already inspired the development of many biologically inspired SLAM algorithms such as NeuroSLAM and RatSLAM [2–4]. These have shown the advantages of needing fewer sensory inputs such as lower resolution visual inputs thus less computation power required than conventional visual-based SLAM algorithms. NeuroSLAM shows promise of performance comparable to that of living organisms, surpassing the current computation-heavy algorithms. Yet problems arise when implementing such models since most of them encode behavior spatially, resulting in complex mathematical computations that must then be implemented in the hardware [12]. This behavior model abstraction fails to take advantage of the elegance and physical properties of underlying neural network circuitry in the hippocampus, resulting in a cumbersome implementation and failing to sufficiently reduce the resource demands to match those typical of a neuromorphic system, whether implemented in software or hardware.

To approach the efficiency of the brain and the understand on brain's mechanism of localization and navigation, we choose to build a neuromorphic system consisting of the underlying neurons and networks that performs path encoding and integration. We want to generate the spatial encoding neurons, i.e. place and grid cells, from the movement encoding cells from a designer's perspective to gain insights on the challenges of neural non-uniformity and network complexity. We believe that the remedy we proposed to these challenges would provide interesting hypotheses on the neural network's topology of brain's navigation system and functionality of grid cells, which do not provide direct mapping of space.

Models of how spatial encoding neurons—i.e. the place cell and grid cells—are emerged from neural networks have been proposed. Many of the attempted models fall into two main categories: continuous attractor networks (CANs) [13–15] and oscillatory interference (OI) [16–18] models. In CAN models, grid-cell patterns emerge from a network in which each cell has a recurrent connectivity with its neighbors. Each cell has a characteristic preferred direction, meaning that the cell tends to fire more rapidly when the animal is moving in that direction. Each of the cells projects weighted connections, with an inhibitory center-surround circular weight profile, to its neighbors and receives inhibition and excitation from others as well. The local maxima then translate as the animal moves, creating a grid-cell firing pattern [13–15]. The OI model is radically different. It forms grid cells by interfering oscillators, with frequency controlled by the animal's locomotion velocity, and encodes the path integration into phase accumulation of the interference results.

In 2016, Welday observed such velocity encoding cells and named them as 'theta cells' [19].

Both models provide challenges for hardware implementation. CAN models are network population models that require large numbers of connections between their constituent neurons for their recurrent network to function. Furthermore, the weight profile contains excitatory and inhibitory weights that are computed based on distance to neighbors, aside from receiving excitatory input from movement encoding neurons, increasing the computational complexity of a programmable network implemented in hardware. The OI models are much simpler in terms of their modularity since each grid cell receives feedforward excitatory signals from oscillatory cells such as the theta cells. Yet, due to their phase accumulation principle, OI models require an accurate frequency relationship with velocity and uniformity of its constituent oscillators, which is unrealistic considering the mismatch between either analog VLSI circuitry or biological cells.

The implementation of the fundamental block, i.e. the theta cells, poses difficulties as well. Our team's previous work has shown that it would be difficult to maintain the oscillation's stability while maintaining its sensitivity to velocity inputs due to its complex ring attractor structure [20]. To amend this problem, we designed a theta chip that employs the principle of abstract neuromorphism to implement the theta cells' behavior model by exploiting the simplicity of analog computation circuitries. We published an early design for the chip in [21] and then taped out the chip in the TSMC 65 nm process. In this paper, we will briefly introduce the final design of the theta chip in section 3, and its performance and proposed application in implementing place cells in section 6.

If a collection of theta cells is available, it is possible to form neuromorphic grid and place cells as the models suggest. But, as mentioned above, both models encounter hardware implementation problems. In the current stage of our research, we choose to implement place cells based on the OI model's framework due to its simpler network structure and single-cell modularity. To overcome its strict requirements on the oscillators, we previously proposed an improved OI model for neuromorphic implementations that compensates the mismatch between theta cell behaviors with an 'offset reduction' strategy and simplifies the interference operation to logic operations between oscillators with square-wave oscillation profiles. We summarize the principle of the improved model in section 2.2; for a more detailed analysis, please refer to our previous report [22].

Though the model in [22] provides conciseness and feasibility against realistic parameter and behavioral variations, the spatial cell it forms does not replicate the functionality of a place cell. The model is only capable of indicating one segment of a movement rather than tracking the location of the agent throughout a trail. Thus, in this paper, we will refer to the cells formed by the model of [16] as 'egocentric place cells'. They are egocentric due to their response region, or place field, are centered in a coordinate system that moves along with the animal, while the original place cells are fixed in the world coordinate system. The model in [22] proposed a vector accumulation strategy for localization by resetting the egocentric reference frame according to the firing of egocentric place cells. Here, we realize that concept by proposing a place cell network model that receives input from the egocentric place cells and accumulates the movement in a neuromorphic fashion. We describe the structure of the place cell network in section 5 and how it reacts to implemented egocentric place cell signals in section 6.3.

Thus, in this paper, we demonstrate the results of a hardware implementation of place cells that can track a robot's location. Place cells are obtain from networks of egocentric place cells implemented onto a Spartan-6 FPGA with the theta cell signals from a mixed-mode theta chip. The network structure is computed through our proposed neuromorphic model. The results show that the place cells can be generated from a simple feedforward network with logic node operations from a group of theta cells that are not uniform in behavior. This work proves the feasibility of an efficient neuromorphic SLAM system with place and grid cells generated from a biologically plausible and simple network while providing a potential function of grid cells.

2. Methods

2.1. OI model under ideal condition

Part of the model that is implemented is an improvement upon the original OI model, tailored for a more robust and simpler implementation in silicon. It can compensate for the inevitable behavioral variations of either biological neurons or neuromorphic implementations while reducing the interference operation to logic operations. The performance and details of the model are published in [22], though we will introduce its basic structure here for completeness. An important characteristic is that to accommodate variations among theta cells readily, the cell formed by the improved model is downgraded into an egocentric place cell reporting segmented displacement rather than being a location-specific cell in the original OI model. In this section, we first review how to form a place cell in the ideal scenario, then discuss why we can get only an egocentric place cell from either the original OI or the improved model. Later in section 5, we will discuss how to integrate the segmented displacement into localization with respect to a global reference frame.

As predicted by the OI models [16, 17], the fundamental components of an OI model are oscillators that can encode the animal's moving velocity into frequencies. Then the integration of velocity can be translated into the accumulation of angular velocities, thus achieving path integration for localization. This type of neurons was later observed and reported in [19] with their oscillatory behavior is related to the animals' traversing velocity as described in equation (1)

$$F = F_{\text{idle}} + \beta\left(\vec{V}\cdot\vec{V}_{\text{p}}\right) \quad . \tag{1}$$

Here, F is the oscillation frequency of a theta cell. It is centered at a constant idling frequency F_{idle} and modified by a scaled inner product between its preferred direction unit vector $\vec{V}_{\text{p}}$ and the agent's velocity $\vec{V}$. The scaling coefficient β is the gain or frequency response factor. The parameters β and F_{idle} are relatively stable for one theta cell but differ between theta cells as Welday *et al* discovered [19].

In the OI models, grid cells and place cells can be obtained by interfering with various theta cells [16, 17]. First, spatially periodic bands or gratings can be formed by interfering a theta cell with a cell that has an oscillation frequency at F_{idle}, with the results shown in subplots (a)–(c) of figure 1. The process resembles the down conversion from the demodulation of wireless communication to remove the 'carrier frequency' F_{idle} then extract the $\beta(\vec{V}\cdot\vec{V}_{\text{p}})$ term that encodes spatial information. The resulting signal is the cosine of the phase accumulated by the moving velocity projected onto the preferred velocity of the theta cell. Thus, its spatial firing pattern forms a periodic sinusoid along its preferred direction. The difference in periodicity of subplots (a)–(c) in figure 1 is due to distinct scaling coefficient β, or the magnitude of the theta cell's preferred velocity vector. Grid cells can be formed by interference between gratings of preferred direction that are multiples of 60° apart, as indicated by the red dotted arrows in figure 1. Place cells can be formed in a similar fashion but with gratings with a much larger period, which can be obtained through interference between denser gratings but with mutually prime scaling coefficients, as shown by the green arrows in figure 1.

2.2. Improved OI model with theta cell variations

The improved OI model employs a similar interference structure in general but discovered several realistic factors that lead to the improvements and alternation from place cells to egocentric place cells. In an analog

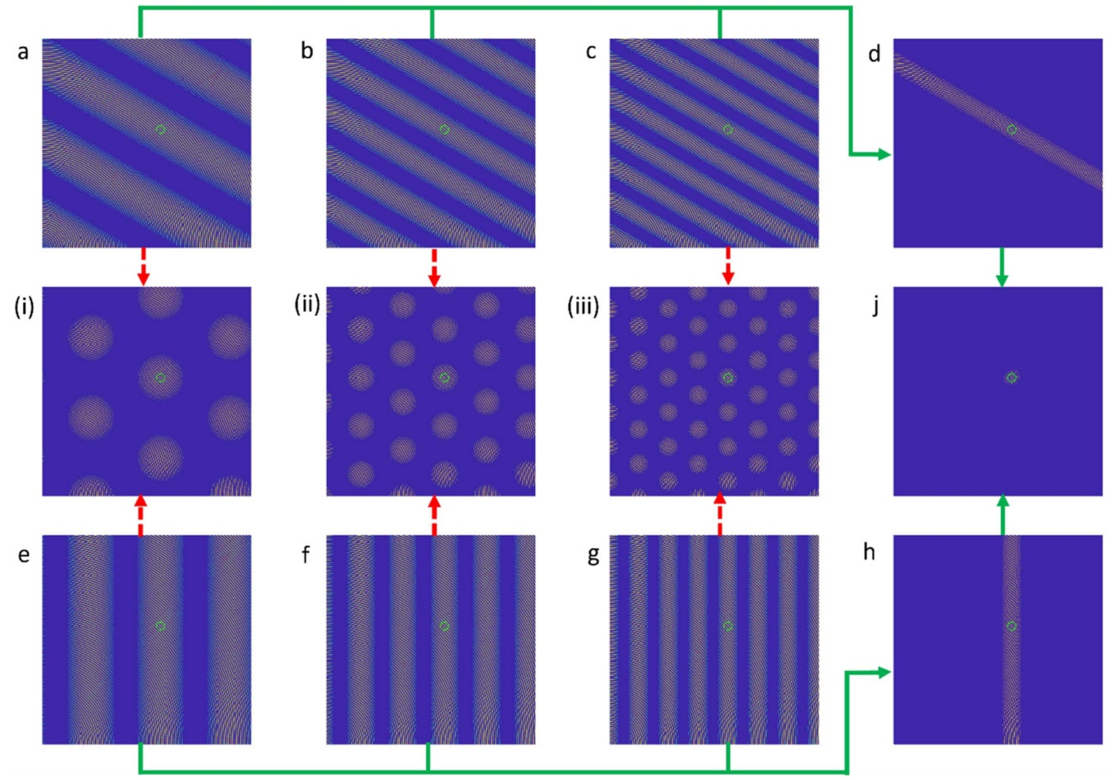

Figure 1. One method to form a place cell in the ideal scenario: Two groups of theta cells, denoted (a)–(c) and (e)–(g) interfere with a reference theta cell. Both groups have the same set of mutually prime frequency response factors, but with their individual preferred directions 120° apart. A place cell can be formed along the pathway indicated by the green arrow: first, a single stripe is formed, and this is intersected by another at a desired location, marked by the green circle in (j). Alternatively, grid cells (i)–(iii) can be formed by following the red dotted arrows, then interfering the hex grids to form the same place cell in (j). This is a reproduction of figure 5 in [22]. Reproduced from [22]. © The Author(s). Published by IOP Publishing Ltd CC BY 4.0.

implementation or a biological neural circuitry of a theta cell, it is unlikely that all theta cells share the same baseline frequency F_{idle}. Even with a distributed pairing strategy, the chance of finding two theta cells with the exact same F_{idle} is minimal. Here in equation (2), we denote the term F_{off_n} as the offset frequency for the nth theta cell with respect to an average baseline frequency among all theta cells

$$F_n = F_{\text{idle}_n} + \beta_n \left(\vec{V}\cdot\vec{V}_{pn}\right) = F_{\text{idle}} + F_{\text{off}_n} + \beta\left(\vec{V}\cdot\vec{V}_{pn}\right) \quad . \tag{2}$$

In the improved model, with schematics on the bottom of figure 2, an offset-reduction strategy is proposed to reduce the impact of this offset term by interfering between theta cells that have similar F_{off} but opposite preferred directions. We model the logic *AND* interference operation as multiplication here with operation symbol $\otimes$ to indicate that only the low frequency component is considered. The following equation demonstrates the effect of the interference in the signal domain. The actual oscillating signal of any theta cell contains an initial phase φ_i, which is critical to determine the location of the place field in the OI model for place cells

$$\begin{aligned}
&\cos\left(2\pi F_a t + \varphi_a\right) \otimes \cos\left(2\pi F_b t + \varphi_b\right) \\
&\quad = \cos\left(2\pi\left[\left(\beta_a\left(\vec{V}\cdot\vec{V}_{\text{pa}}\right) + F_{\text{idle}} + F_{\text{off}_a}\right) - \left(\beta_b\left(\vec{V}\cdot -\vec{V}_{\text{pa}}\right) + F_{\text{idle}} + F_{\text{off}_b}\right)\right] t + \left(\varphi_a - \varphi_b\right)\right) \\
&\quad = \cos\left(2\pi\left[\left(\beta_a + \beta_b\right)\left(\vec{V}\cdot\vec{V}_{\text{p}}\right) + \left(F_{\text{off}_a} - F_{\text{off}_b}\right)\right] t + \left(\varphi_a - \varphi_b\right)\right) .
\end{aligned} \tag{3}$$

This operation suppresses the phase error accumulation. Notice that the result has a very similar mathematical form and spatial pattern as the original theta cell, with a new frequency response factor $\beta = (\beta_a + \beta_b)$ and a new offset frequency $F_{\text{off}} = F_{\text{off}_a} - F_{\text{off}_b}$. Furthermore, the summation of frequency response factors $(\beta_a + \beta_b)$ makes the $\vec{V}t$-dependent term in (3) more dominant than the subtracted offset frequency, with the effect shown in subplots (a)–(c) of figure 2. Because of the similarity in behavior, we can view the result as an effective theta cell. This modularity of the offset reduction strategy enables a layered

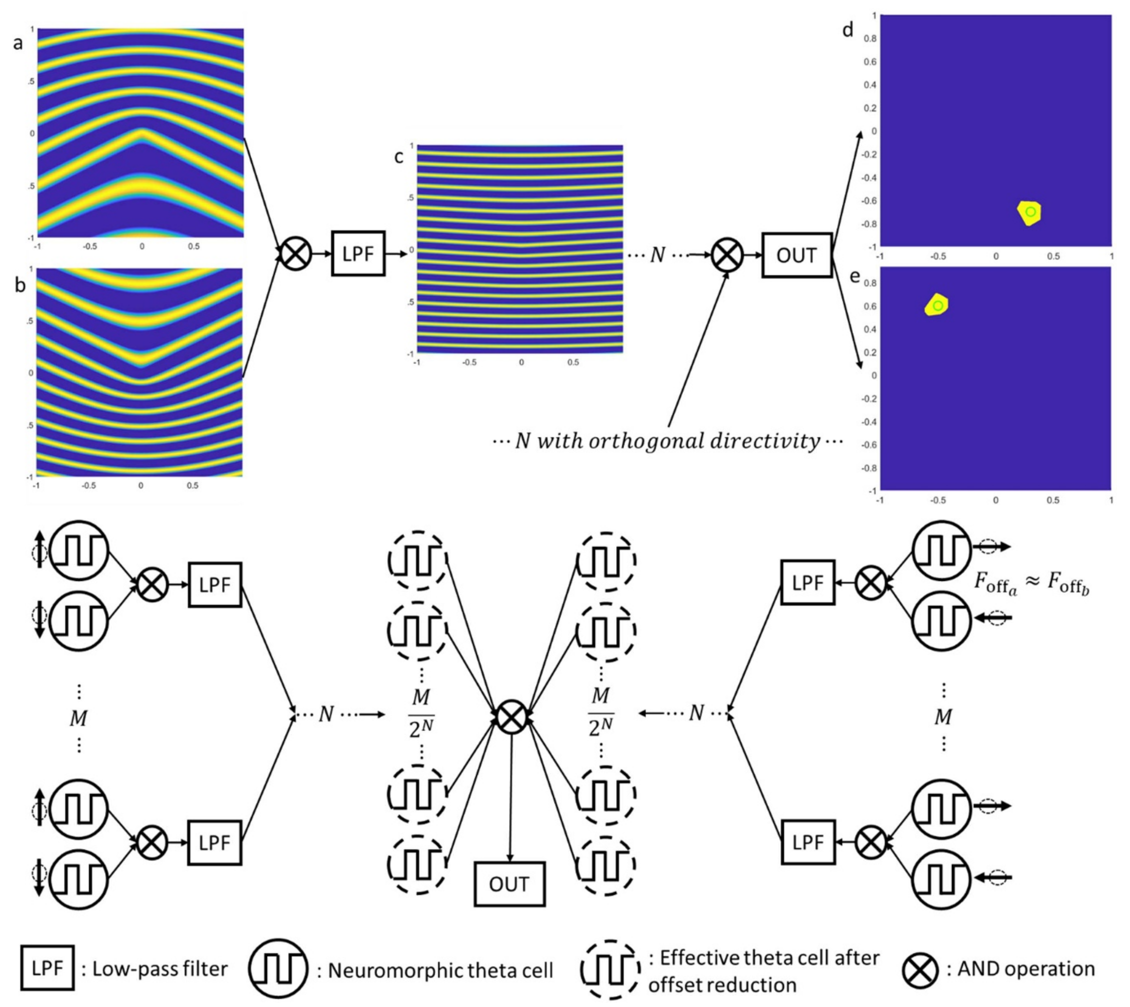
a
b
c
d
e
1
.5
0
.5
-1
-0.5
0
0.5
0.8
0.6
0.4
0.2
-0.2
-0.4
-0.6
-0.8
LPF
OUT
··· N ···
··· N with orthogonal directivity ···
M
$\frac{M}{2^N}$
$F_{\mathrm{off}_a} \approx F_{\mathrm{off}_b}$
LPF : Low-pass filter
: Neuromorphic theta cell
: Effective theta cell after offset reduction
: AND operation

Figure 2. Subplot (a)–(c) shows the effect of the offset-reduction method. (a), (b) are the spatial response of two interfered theta cells with $\beta = 3.5$ and 4.9, $F_{\mathrm{off}} = 10$ and 13.5 relative to the reference frequency, and preferred directions of 0° and 180°. Subplot (c) is the result of interference between the two theta cells directly; boosting β results in a denser grating and less F_{off} to straighten the stripes. Subplots (d), (e) are sample egocentric place cells formed by a group of 48 theta cells with a 25% relative standard deviation on idling frequency and a 20% relative standard deviation of frequency response factor β. Bottom: Schematic of the offset-reduction method to form egocentric place cells with theta oscillators with variations in β and base frequency and non-zero F_{off}. Figure from figure 8 of [22]. Reproduced from [22]. © The Author(s). Published by IOP Publishing Ltd CC BY 4.0.

structure as shown in the schematic in figure 2, should the variation be large. This strategy also eliminates the need for idling oscillators and consists purely of theta cells, further reducing system complexity. The variation in β among theta cells is less of a problem since it contributes to the uniqueness of the egocentric place's firing field, similar to the method of spacing by mutual primes discussed previously. The uniqueness problem is a more predominant issue due to our simplification that converts the sinusoidal oscillation profile of theta cells to square-wave since it basically regularizes the positive part of a sinusoid to one. Please refer to the original publication [22] for a more detailed discussion. In conclusion, the variations in both β and F_{off} becomes advantages when forming a unique firing field for place cell while applying a square-wave oscillation profile, enabling us to use logic *AND* operation for interference to save resources.

In the actual scenario however, we understand that the offset frequency F_{off} cannot be eliminated all the way to zero, so the phase shift computation must be adjusted as in (4) due to the remaining offset frequency, even after offset reduction. The modulo operation is to account for digitized phase shift in an implemented system, such as a ring oscillator described in the next section that offers 8 digitized phase shifts, or a neural circuit model of theta cell in the form of a ring oscillator [20, 23]

$$\varphi_i(R,\theta) = \mathrm{mod}\left(1 - \mathrm{mod}\left(R\left(\cos\left(\theta - \theta_{\mathrm{p}i}\right)\beta_i + \frac{F_{\mathrm{off}_i}}{|\vec{V}|}\right), 1\right), 0.125\right) \quad . \tag{4}$$

Here, φ_i is the phase shift of the ith effective theta cell after our proposed *AND* interference for the egocentric place cell designated for location $\vec{x}$. R and θ are the polar coordinates for $\vec{x}$, and $\theta_{\mathrm{p}i}$ for $\overrightarrow{V_{\mathrm{p}i}}$. The spatial firing patterns of two egocentric place cells with arbitrary designated locations are shown in figures 2(d) and (e). The modulo 0.125 operation is to accommodate the eight-phase digitized output of the theta chip, which will be introduced in the next section. They are formed from the same group of 48 simulated theta cells with a 25% relative standard deviation on idling frequency and a 20% relative standard deviation of frequency response factor.

The reason for the degradation from place cell to egocentric place cell is because of the remaining F_{off_i} term. They only operate when the theta cells are all in a known state and the agent is traveling with a constant velocity when reaching any point in the spatial maps of figure 2, due to the phase accumulated through $F_{\mathrm{off}}t$. A phase reset procedure is proposed in [22] to address this problem. The procedure is triggered either 1: at a fixed interval when velocity is constant or 2: in the event of changing the movement velocity. The first condition is to clear unforeseen errors, such as thermal noise or crosstalk, accumulated by regularly pulling the system back to a known state. The second condition is due to the dependence of phase accumulated with time induced by the remaining offset frequency, generating a path dependency from the origin to any point. For example, the agent can travel from the origin to [1,1] directly, or by detouring via [1,0]. Though both paths end at the same location, the difference in travel times leads to different phase accumulations across the theta cells. Thus, each segment of the path must be recorded as a displacement vector, triggering the phase reset event and creating a new egocentric frame at the point of velocity change. Every time the phase reset event happens, the system can record the current egocentric place cell firing to achieve a path integration or, in other words, a dead reckoning. In section 5 of this paper, we describe our proposed model for place cells to perform localization through the accumulation of egocentric place cell activities.

3. Theta chip

3.1. Design of the theta chip

A theta chip has been designed and taped out with TSMC 65 nm technology, targeted at producing the behavior described by equation (1). Though a neural attractor network model was previously proposed in [20], it consists of many neurons with both inhibitory and excitatory interconnections, making VLSI implementation and configuration difficult. In order to provide an array of programmable theta cells with reasonable hardware resources, we choose to implement the theta chip with abstract neomorphism by reproducing the theta cells' behavior model. But, to preserve an analogy to the neuronal behavior, we employ a mixed-mode design with analog computation circuitry to reduce transistor count as well as a continuous-spectrum response to the input velocity. We also choose digital output for the theta unit oscillations for easier handling by external components. We briefly describe the final design of the chip below; a detailed description of an early design of the included circuits is discussed previously in [21].

The chip consists of 128 theta cell units with an I/O (input-output) arbiter for the control, program, and output of the theta units. Each theta unit has an individually programmable preferred velocity and operates asynchronously. A theta cell unit includes four major components.

(1) SRAMs: Each unit has two 4-bit SRAMs to store the x and y components of the preferred velocity $\vec{V}_{\mathrm{p}}$. The values are signed and in ascending order with value 8 (binary: 1000) representing the zero value. They can be programmed during the chip's start-up phase.

(2) A/D Converters: Since the preferred velocity vectors are not to be changed after configuration, capacitance DACs that require refreshment are not preferred here. We adopted a W-2W transistor ladder [24] with a long transistor length to minimize current consumption. Two such DACs are implemented for each theta unit, connecting to the preferred velocity SRAMs.

(3) Analog Computation Module: The analog computation unit calculates the inner product between the theta unit's preferred velocity and the input movement velocity. We use two Gilbert cells to compute a continuous four-quadrant dot product between the internal preferred velocity and the movement velocity input to the theta unit, both represented in analog voltages. The Gilbert cells require less power and fewer transistors than conventional multipliers. The analog multiplication generates a pair of differential voltages as the product. Two pairs of differential voltages, representing the products of the x and y components, are converted into two currents using differential pairs, and the sum of the two currents represents the dot product, as shown in figure 3(c).

(4) Oscillator: The basic structure of the oscillator is a current-starved ring oscillator as shown in figure 3(b), where the control current for the ring oscillator is mirrored from the dot product circuit. An extra NMOS transistor is added between the inverters to allow a manual hold for the oscillation with the control signal Cap_clear, the model needs this phase reset capability for pulling the oscillation to a known phase for correcting accumulated error. To achieve a linear relation between the current and frequency, as well as to reduce the oscillation frequency, extra load capacitance is introduced between inverter stages. Eight of the nine inverters are connected in parallel with a delay capacitor taking

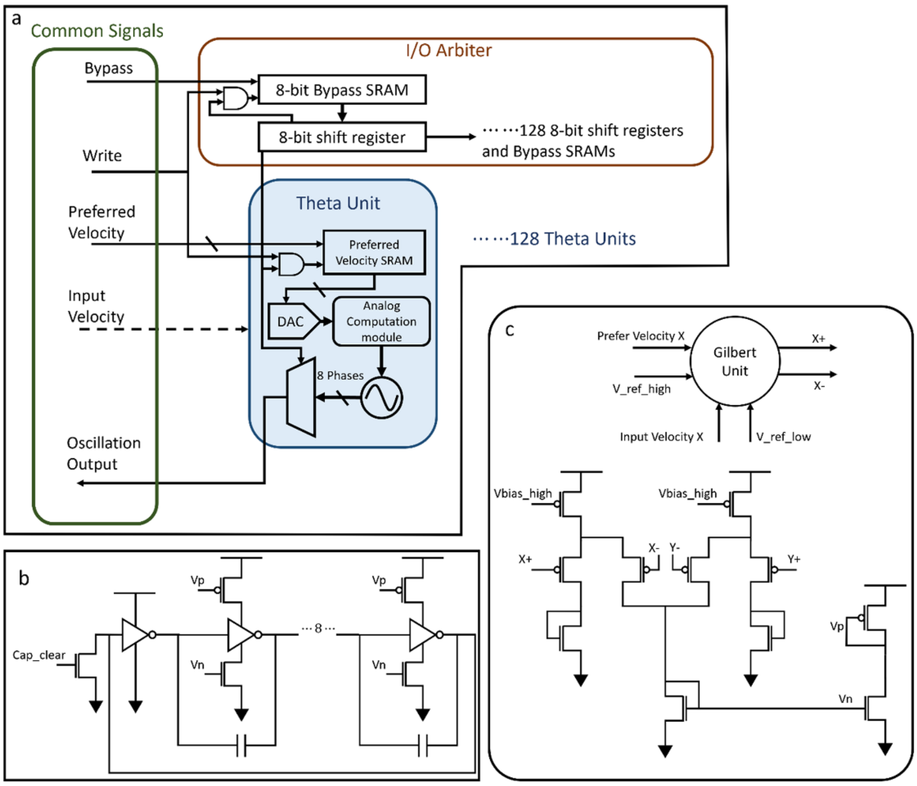

Figure 3. Theta cell schematics: (a) general arrangement of the theta chip. The green 'Common Signals' box on the left shows all the broadcasting control and input signals to all theta units, with one shared oscillation output port. A shift-register based I/O arbiter, with bypass capability, is responsible for indexing each theta unit for initial configuration and oscillation output during operation. The theta units store the programmed preferred velocity and perform real-time computation of equation (1) through the analog computation module shown in box c, then regulate the oscillator shown in box (b). (b) A 9-stage, current-starved ring oscillator with reset capability. (c) The analog computation module performs the multiplication using a Gilbert cell and then computes the summation in current mode to achieve vector projection.

advantage of the Miller Effect, thus ultimately reducing the capacitances needed down to 1 pF each. This design provides a digitized eight-phase output of each theta cell unit for the improved OI model to choose from through equation (4). And, since the TSMC technology provides metal-metal capacitors in upper layer metals, the capacitors are placed above the transistors to reduce the area needed for the entire design.

The I/O arbiter follows the concept of Time Division Multiple Access for the I/O of each theta unit, according to the schematic shown in figure 3(a). It comprises a chain of 1024-bit shift registers that forms 128 groups of 8-bit registers. Within the group, each bit enables one phase output of a theta unit, and the first bit also provides an enable signal for programming the preferred velocity SRAM of this unit. Each register is accompanied by a bypass SRAM that determines whether the shift path goes through the register or bypasses it. The bypass capability allows a shorter scan cycle after the calibration and can only provide signals that are useful for further processing. Upon start-up, the shift register will shift through all the theta units and their 8 phases to program each theta unit's preferred velocity and the Bypass SRAM for each phase output.

3.2. Operation of the theta chip

The chip is placed on a custom PCB to interface its digital ports with the FPGA and to meet its analog bias requirement by a DAC. The chip employs serial input and output. Preferred velocity input is transmitted over an 8-bit bus with the lower 4 bits carrying the x component value and the upper 4 bits for y. Upon startup, the clear signal needs to be held high for a few clock cycles to guarantee reset of all SRAMs and shift registers. The first bit of the long shift register will be held high to index the first theta unit's preferred velocity SRAM and the Bypass SRAM for the first phase of the oscillation output of this unit. Then if pulling the active high enabling signal Write, the data input signal bypass and the preferred velocity byte can then be used to program the theta unit's output and preferred velocity. Each clock pulse proceeds the shift register to program whether to output each phase of an oscillation, and every eight clock pulses will move the index to the next theta unit, eventually looping through all 128 units. After the initial setup, the clock then only scans through the phases that are programmed to be output, reducing the length of the scanning cycle or, equivalently, increasing the sampling frequency without increasing the clock frequency. The user can then load the moving velocity of the agent either digitally through the preferred velocity byte by pulling load signal high, or through analog voltage using two analog input pins.

4. Egocentric place cell implementation

4.1. Configuration of the egocentric place cell network

As suggested by the improved OI model, the first layer of interference should be between theta units with similar F_{idle} but with opposing preferred directions for offset reduction. The total number of layers needed depends on the distribution of F_{idle}. In this demonstration, we implemented only two layers to show the capability of our model with a small number of operations. In figure 8 in the results section, 82 of the units exhibit a coefficient of determination higher than 0.9. Thus, the structure of a two-layered network will have 40 interference pairs in the first layer and 20 pairs in the second. Among the participating 80 units, units are paired to have the closest possible idling frequencies. The output node will be the direct logic AND operation on the outputs of the 20 nodes of the second layer, with the structure shown in figure 4.

Since the velocity is represented in Cartesian coordinates, the straightforward choice of preferred directions for the theta cells are positive and negative directions along the x and y axes. Given the programmability of the theta units, we can first form 40 pairs based solely on the closeness of F_{idle}, then assign 20 pairs with opposing velocities along the x axis, and the other 20 along the y axis. In each pair, for example, one theta unit might be programmed to have a preferred velocity of [4, 0] and the other with [−4, 0]. In the second layer, we can choose to interfere between one from the x-aligned group and one from the y-aligned group. This operation resembles the formation of grid cells as shown in figure 1(i-iii), showing that one potential functionality of the grid cells is to reduce the influence of offset frequency. An alternative is to repeat the process for pairing based on the similarity of frequencies. Thus, the network consists of 60 interference operations, each of which comprises a logic AND between two signals and a low-pass filtering process as illustrated in figure 4, which is an instantiation of figure 2 but with an inherent formation of grid cells.

4.2. Egocentric place cell network implementation

The network for the egocentric cells is implemented with the Xilinx Spartan-6 FPGA. As shown in figure 4, the implementation comprises two main components: an interference node and a multiplexer. Each node contains simply an AND gate followed by a filter to remove the high-frequency component as suggested by the models. In systems like biological neural networks or similar neuromorphic network systems such as IFAT [25–27], integrators like the neuron's cell membrane or a capacitor for an integrate-and-fire neuron model can perform this low-pass filtering. In our current implementation in the FPGA, we mimic such functionality through a 9-tap Hamming window function followed by a digitized RC circuit. And, to show the compatibility of the system's filters, the filters in the second layer of nodes use a 9-tap moving average filter with a digitized RC circuit with a larger time constant. All the filters are arranged in a pipeline to ensure a continuous data flow and to allow the network output to be synchronized with the clock. The output node, which is simply a 20-input AND gate, produces the output of the place cell which is then buffered in a FIFO queue for streaming to a PC for the next layer, as will be described below.

The multiplexer in figure 4 interfaces between the theta chip and the network described above. For efficiency, the data path structure between network layers is fixed, thus localizing the job of network configuration to the first layer's input. It scans a cycle of the theta chip and directs each oscillation output to its position in an 80-bit wide buffer based on a lookup table, whose values are computed from equation (4) with the frequency information obtained from a calibration cycle. After the multiplexer finishes each scan cycle, it generates a clock signal for the network to load in the 80-bit buffer and advance the interference process.

4.3. Interfacing between the theta chip and the network

As described above in section 3.2, the network in the FPGA needs to initialize the theta chip before operation. Based on equation (4), a place cell's designated location is determined by the initial phase shift relation among the theta cells. Combining that outcome with equation (3), every interference result is the difference between the initial phases of the source signals. Thus, in our 2-layered network, the output of the second layer depends on the initial phase of 4 signals. If we initialize 3 of the signals with the same initial phase, the difference between the initial phase of the fourth theta cell with the other 3 can determine the initial phase of the node of the second layer. So, the number of phases to be output by the theta chip is programmed to be $60 + 8 \times 20 = 220$, where one of every 4 theta units has all 8 phases available for the multiplexer, denoted as the 8 dots around one theta unit in figure 4. After the theta chip is initialized, we gather the traces for the 80

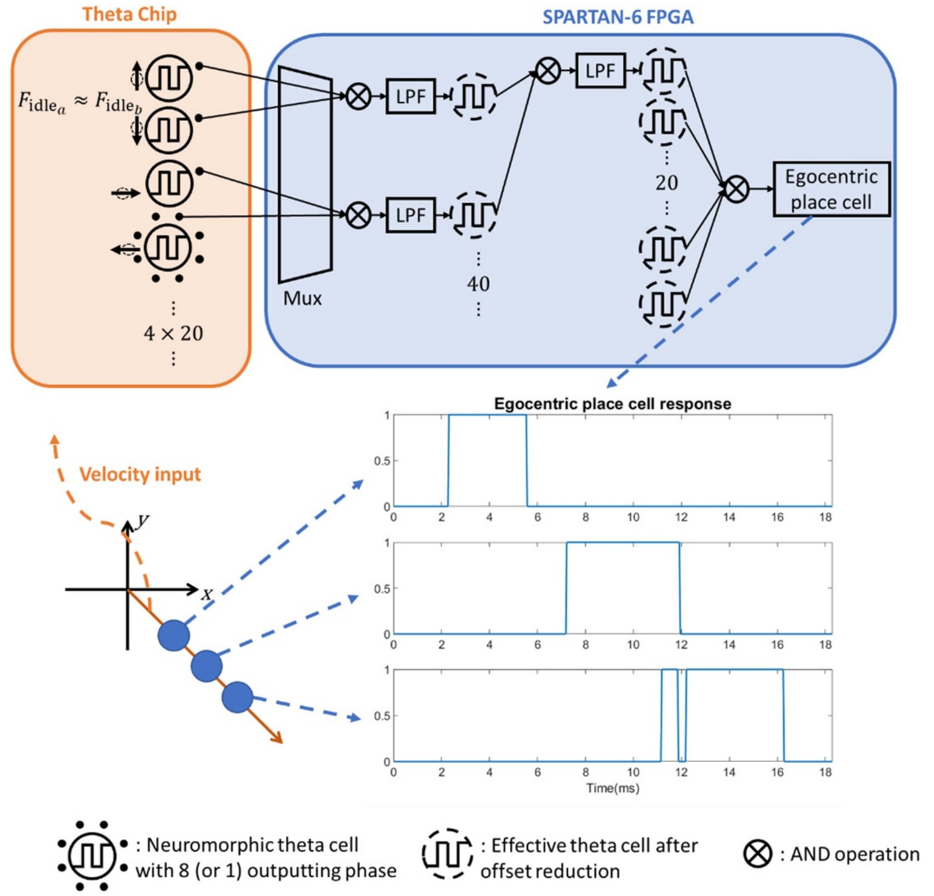
Theta Chip
$F_{\text{idle}_a} \approx F_{\text{idle}_b}$
4 × 20
SPARTAN-6 FPGA
Mux
LPF
LPF
LPF
40
20
Egocentric place cell
Egocentric place cell response
Velocity input
y
x
Time(ms)
: Neuromorphic theta cell with 8 (or 1) outputting phase
: Effective theta cell after offset reduction
: AND operation

Figure 4. Implementation schematic of the egocentric place network. After a certain velocity is asserted to the theta chip, theta units' oscillations are directed to the input layer of the egocentric place network by a multiplexer based on a lookup table. Below the schematic are three representative egocentric place cells implemented along the same direction and related output response.

theta units and compute their frequency to compute the phase connection lookup table, given the desired location of a egocentric place. In this form, any egocentric place (allowing for digitization error) within the range can be generated with the same basis of 220 theta phases by a different lookup table for the multiplexer. Their results for tracking the movement within a certain range are demonstrated in figure 10 in the results.

5. Place cell network

Though the egocentric place cells we implemented above can perform basic tracking functionality [22], they do not provide a one-to-one encoding of space as typical place cells are observed to do. And, as stated in [22], a location can be encoded by a certain sequence of firing from such cells. In other words, they function as basis vectors. To realize the spatial encoding capability of place cells, we add another layer of cells that functions as accumulators to represent the vector summation. The structure of this layer is shown in figure 5. Here, a set of self-recurrent place cells are indirectly connected with its neighbors through path cells. The path cells operate like unidirectional switches or AND gates controlled by the egocentric place cells. When an egocentric place cell fires, the path cell that is enabled by an activating place cell is triggered to excite the next place cell while turning off the self-excitatory loop of the current place cell to ensure the transfer of the activity bump. Then, a leakage process is also simulated to discharge the activity of the previous place cell back to baseline level. An alternative way for implementing the transfer of activity bump, especially in the case of actual neural circuits, is to replace the gating of self-excitatory loop by inhibition connections between adjacent place cells. Given the neural firing property of spike rate adaptation, the newly activated place cell would have a spike frequency higher than the previous one thus able to inhibit it back to baseline level thus ensuring the uniqueness of the activity bump after the transfer occurs.

This structure loosely resembles the CAN model of place cells in which the localization manifests in the migration of activity bump. The main difference is the lack of direct connectivity between the place cells and the homogeneity among place cells; both drastically reduce the complexity. We believe that the connection between place cells can be used for path planning and navigation but is not necessary for localization, as we

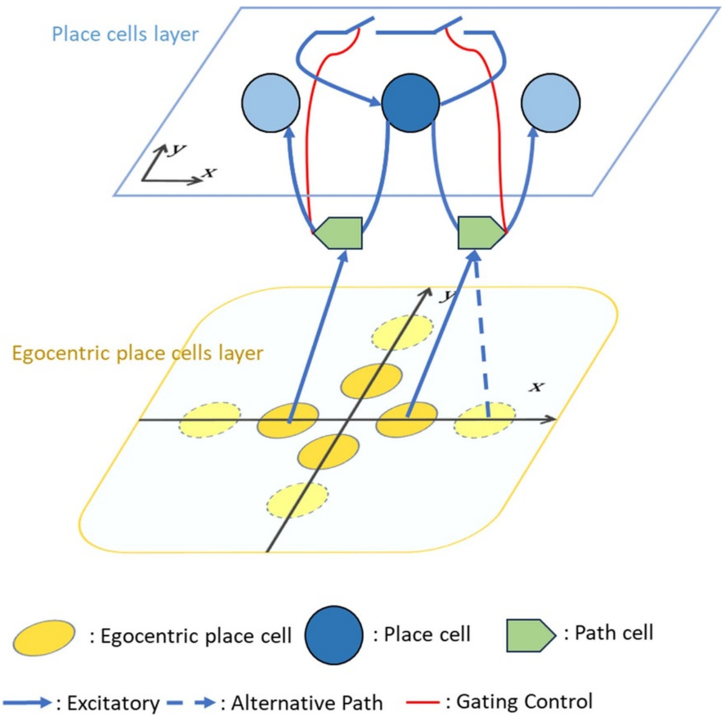

Figure 5. Place cell network structure for path integration. Each place cell is connected to its neighbors through path cells (y-direction place cells are omitted for clarity) that are gated by the egocentric place cells. When a path cell fires, it transports the activity from the current place cell to its corresponding neighbor and shuts the self-excitatory path off. All sets of path cells can be connected to the same set of egocentric place cells. Here, the path cells are connected to the inner circle of egocentric place cells to create a homogeneous map with small scale. A dynamic map can be formed by using egocentric place cells with different magnitudes, as indicated by the faded egocentric placer cells and dashed connection.

have not included it in the model under consideration here, further description will be postponed until the Discussion. The path cells replace the activity bump transfer functionality that is realized by the asymmetric inhibition profile between place cells and different directional preferences among the place cells in the CAN model. Thus, each place cell is modularized into the structure shown in figure 5. This modularization allows an expandable and concise implementation scheme, in contrast to the original CAN model's requiring a substantial number of cells within each patch of the network [13–15]. The path cells outsource the need for directional preference cells to the egocentric place cells which, in turn, can be centralized to save resources that are needed by the reduction of theta cell variations as discussed above and in [22].

Overall, our place cell model greatly simplifies the CAN place cell network by eliminating the complex weight profile between place cells and, thus, the population nature of the attractor networks [13–15]. Moreover, interesting capabilities can be achieved when exploring the connections between path cells and egocentric place cells. For example, if the path cells tap into a different set of egocentric place cells with a different magnitude, the sheet of place cells can be reused to form a space with a different resolution and scale, and similarly for orientation. Furthermore, if we assume learning and plasticity abilities of individual path cells, the map learned by exploration may have a dynamic and inhomogeneous spatial encoding based on the density of the external events and the complexity of the path, opening possibilities for more efficient and dynamic mapping and navigation strategies such as quadtree mapping [28]. As mentioned previously, a phase-reset signal is needed to start the next segment of tracking. In the current setup (figure 5), the reset signal is issued by the firing of any involved egocentric place cells, indicating the end of the current tracking segment.

6. Results

6.1. Theta chip

After we received the theta chip from TSMC then placed on a testing PCB to interface with the FPGA asshown in figure 6, We first evaluate the theta chip for its accuracy in reproducing the oscillation frequency behavior described in equation (1). To have a more thorough evaluation of the performance, we supplied analog voltages that override the internal DACs for digital inputs. As a few units' responses shown in figure 7, the frequency demonstrates a sigmoid relationship with the inner product value. Thus, during the operation,

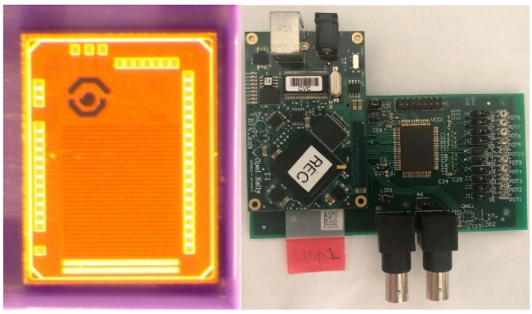

Figure 6. Left: A photo of the theta chip's die. The left column of pads are digital I/Os and the right-column pads are for analog bias inputs. Right: The top board is a SPARTAN-6 FPGA connected by standard JTAG jumpers to the bottom board where the theta chip sits.

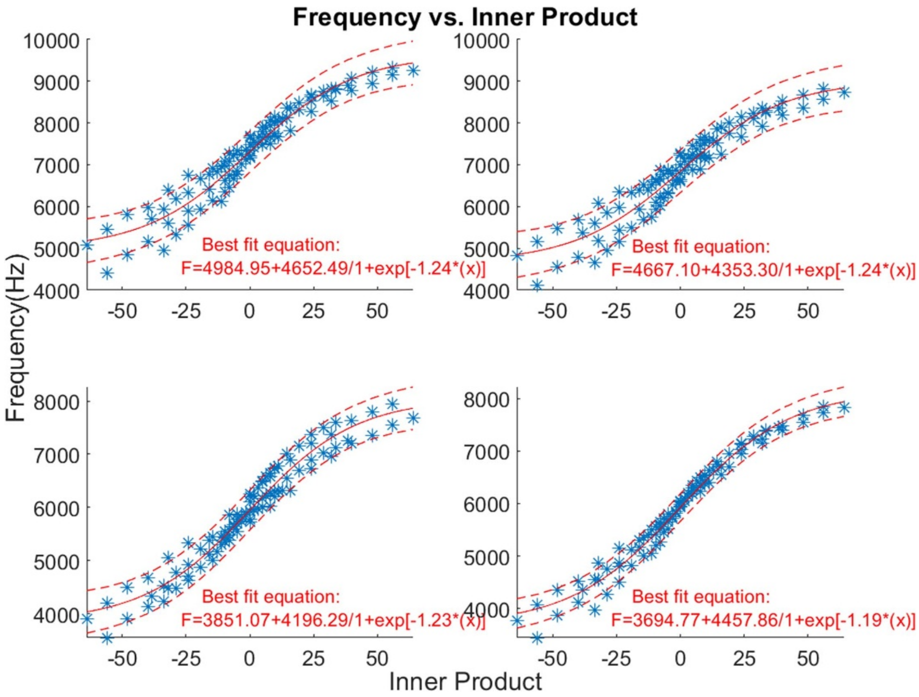

Figure 7. The response of theta units over a larger range of input velocity values. The frequency depicts a sigmoid relationship with the inner product value.

we chose to limit the magnitude of velocities to approximate the linear relationship. The limitation on the range lead to a shrink in frequency swing as well, allowing us to tune down the current supply for the oscillators without concerning them reach equilibrium on deep negative inner product values. This shifts the idling frequency lower from around 6500 Hz–2000 Hz, reducing the power consumption of the chip during actual operation.

The characteristics of the theta chip configured for operation are shown in figure 8. Figure 8(a) depicts a theta cell's selectivity on the input velocity direction. To assess the performance of the theta chip, we exhaustively program all combinations between the preferred velocity and the input velocity for every theta unit, then record the traces. Frequency analysis then gives a relationship between the inner product of the input and preferred velocities with the oscillation frequencies, with a selection of relevant results with actual configuration values used for egocentric place construction are shown in figure 8(b). In general, most of the theta units exhibit a positive monotonic relation between the inner product value and the oscillation frequency. Figure 8 shows a scenario in which the input velocity's *x* and *y* components are scanned separately while the preferred velocity is clamped to zero; it shows that some of the variation comes from the W-2W DAC. A slight offset between the zero value of the DAC output and the broadcasting zero-value reference voltage for the mixer resulted in non-zero multiplication results added to the resultant frequency.

Given the relationship between preferred velocities, input velocities, and oscillation frequencies of the theta units, we fit the data for each theta chip with equation (1) to evaluate their performances. The results,

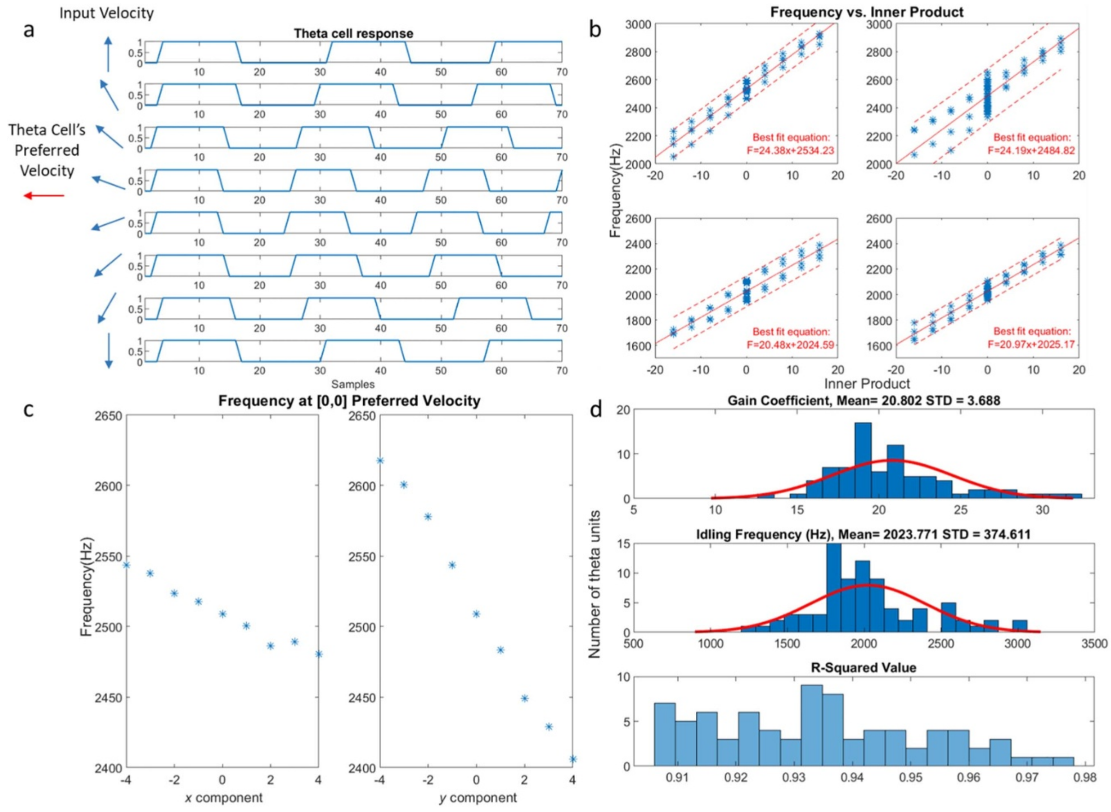

Figure 8. Theta cell characteristic in operation: (a) shows traces recorded from a theta cell when the input velocity's direction swings from +90 to −90° with respect to the preferred velocity direction, demonstrating the realization of equation (1). (b) Shows 4 theta units' frequencies with respect to the inner product and the linear fit of equation (1) with 90% confidence bound. The units' preferred velocities are programmed four times with equal magnitudes but opposite directions along the *x*/*y* direction, which is the configuration further used as inputs to the place cells in the following experiments. They generally depict a linear relationship as expected but have slight offsets for each programmed value. Plot (c) illustrates one potential factor for the distribution of frequency for the same inner product value shown in the upper right subplot in (b). When the unit's *x* or *y* component is programmed to be the zero value (1000 in binary), the frequency still varies linearly with the input velocity's *x* or *y* component. This implies that a difference in voltage between the broadcasting zero-value bias and the internal DAC's zero-value output for preferred velocity forms a small value that still participates in the computation. The DAC's linearity listed in table A.1 provides evidence for this explanation. (d) Depicts the variation in theta cells' parameters after the linear fit to equation (1).

shown in figure 8, demonstrate variations between the units. Later in the implementation, we choose to only use theta units with a correlation of $R^2 > 0.9$. As shown by figure 8(d), the values of β and F_{idle} vary considerably among the theta units due to the analog implementation of the computation unit and the oscillator. As described in section 2.2 and in [22], the variation of β is in fact beneficial in our model since it substitutes the need to deliberately program parallel preferred velocities to be mutually prime. This variation also avoids the need for a very large frequency domain of operation since the magnitude of programmed preferred velocity can be the same across the units, which helps the oscillators to operate without saturating the current starving capabilities of the ring oscillators. Furthermore, the non-uniformity better resembles the biological behavior of neurons and can, therefore, better test the robustness and plausibility of the proposed improved OI model.

We demonstrate the output flexibility due to the bypass functionality of the chip in figure 9. Although the chip's output is serial, by knowing the number of phases programmed to be output, we could re-parallelize the data stream to reconstruct the oscillation of each outputting phase. Figure 9 demonstrates 8 consecutive phases programmed to be output: the first 4 traces belong to different phases of the same theta unit, and the last 4 traces are from different theta units with different preferred velocities. Based on the measurement, an oscillation frequency range between 1500 Hz and 3000 Hz can produce reasonable linearity with the lowest frequency range. Thus, the Nyquist frequency of the scanning clock becomes $(2 \times 4000 \times N)$ Hz, where N is the number of outputting phases. In the experiments, we chose a sampling clock of 6 MHz with 220 outputting phases from the theta chip, resulting in a 27 272.7 Hz sampling frequency for each phase.

To ensure the formation of egocentric place cells, phase accuracy is crucial. In figure 9, we plot the recorded output of a theta unit's 8 phases and the reconstructed signal with the frequency computed from the Fourier transform, and the respective phase shifts digitized at 0.25 π steps. Most of the units show a good correlation between prediction and output. Adaptive algorithms are also applied when configuring the egocentric

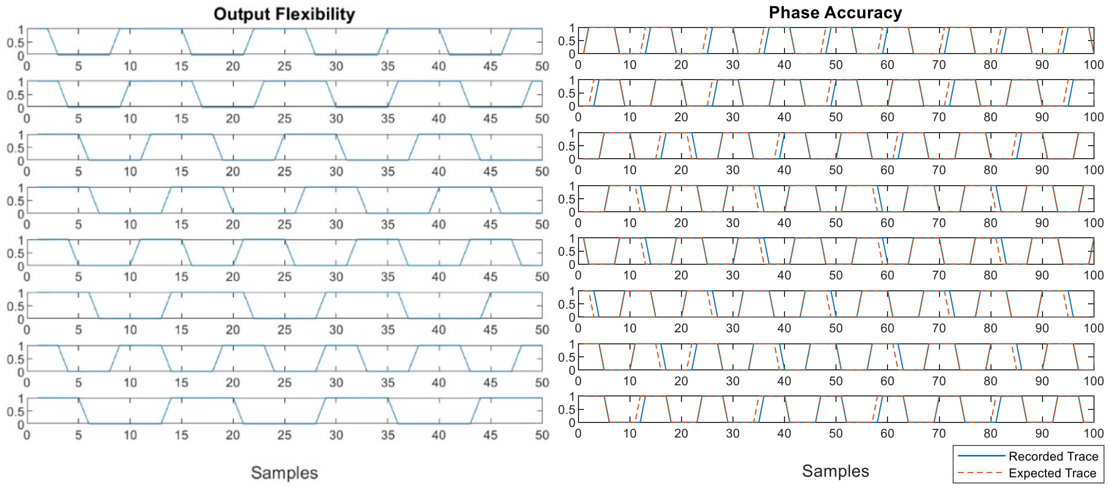

Figure 9. The left subplot demonstrates the output flexibility provided by the bypass function of the theta chip through 8 consecutive traces. The first four traces are from different phases of the same unit, and the last four are from different theta units. The right subplot compares the eight phases from a single theta unit to a simulated reference trace with 0.25 π phase steps. It shows that, in general, the theta units can provide an accurate initial phase value for the formation of egocentric place cells.

place networks to ensure the closest fit between the phase tap and the computed phase φ_i. For cases when the resulted nodes cannot provide constructive interference, eventually, due to cumulative phase alignment error among the participating theta cells, the egocentric place network will simply ignore this group.

6.2. Egocentric place cell network

An instance of the egocentric place network is implemented in the FPGA for validation. We want to test the capability of the egocentric place cells for tracking movements within the domain and the state of aliasing among all the potential egocentric place cells. We generated a grid of 11 × 11 egocentric place cells as the domain, but due to resource limitations on the FPGA, we could only conduct the experiments for each egocentric place within the domain under the same input when building a whole map for the response of all the cells. In other words, the lookup table for each egocentric place is reprogrammed for the same input velocity. The start of each session is signified by the release of the Cap_Clear signal of the theta chip, then we record the network output. A selection of traces is shown in figure 10, where each square shows whether the value of its corresponding egocentric place is high or low. Here, we show snapshots of two trails of the egocentric place cells firing sequentially as the input velocity is held constant. Each egocentric place cell activates only when the agent reaches its place field; this demonstrates its localization functionality. If several of them are deployed simultaneously in combination with the place cell model proposed in section 5, real-time localization can be achieved. Though not shown in the figures, we also observed artifacts from other egocentric place cells coincidentally briefly firing. A similar phenomenon can also be observed in the traces of the relevant egocentric place cells in figure 10, but they are not significant enough to generate a pulse in the subsequent layer since their pulse width are significantly shorter and contains much less energy. Only pulses significant enough would trigger an activity bump migration in the place cell's layer, and thus will not affect the tracking accuracy of the place cells. We have tested various types of window functions with different numbers of orders. Hamming windows with orders larger than 15 can provide egocentric place cell signals with much fewer artifacts. But considering the balance between performance and resource demands for hardware implementation, a 9 tap square window function is chosen. In the experiment shown at the bottom of figure 10, more artifacts can be observed for egocentric place cells with place field further from origin. This is due to the accumulation of unpredictable thermal noise from the theta chip over a longer time. The phase reset mechanism described earlier is intended to restrict the magnitude of noise accumulation and prevent it from getting enough energy to disrupt the tracking in the place cell layer.

6.3. Place cell network

The location tracking mechanism is powered by the basis formed by the egocentric place cells. Though we discussed the potential advantages of an abundant egocentric place basis, the limitation of the FPGA, especially the need for simulated RC filters on board, limits the number of egocentric place networks that can be implemented. As shown in figure 4, implementing just one network requires 80 nodes that each involve a 9-tap FIR and a multiplier for the simulated RC filter. But, since the input is digitized and the FIR is a square window function, the FIR only requires counters. We expect all these excessive components can be easily

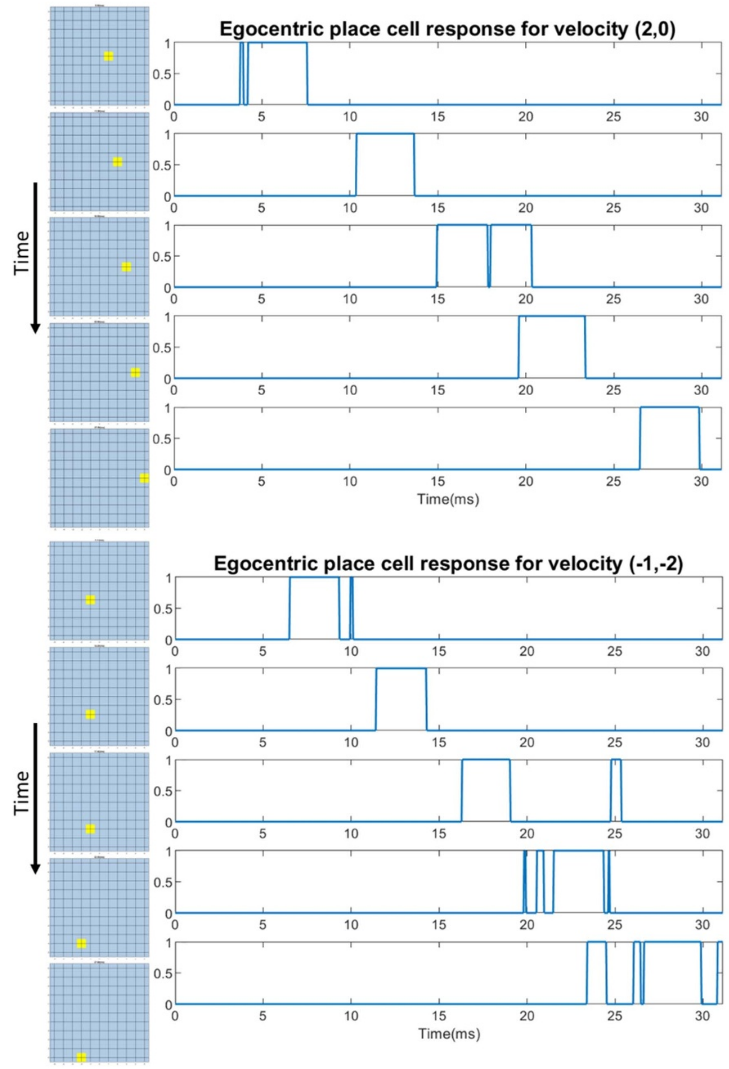

Figure 10. A grid of 11 × 11 egocentric place cells (with digitization) are generated to test the tracking capability of egocentric place cells. The right columns of plot show the egocentric place cells firing as time passes, tracking the agent traveling, with their respective signal traces shown to the right. We can observe artifacts (short spikes in the traces) as well as random flashes from other egocentric place cells, but they are brief enough not to impact the next layer and the major cause is the limited taps of our lowpass filter.

replaced by any existing programmable neuromorphic device that has membrane capacitance imitations such as IFAT, or a mixed-mode ASIC chip, after the system is finalized.

We chose to implement the conventional Cartesian basis on the cardinal directions (N, S, W, E), so 4 such networks need to be instantiated. However, on close observation, due to our 2-layered structure requiring only 1 out of 4 theta cells to have a programmable phase, half of the first layer's nodes are constant and thus can be shared with other vector networks to save resources. In general, the number of sharable nodes is:

$$S = \sum_{n=1}^{N-1} \frac{2^n - 1}{2^N} M = M\left(1 - \frac{N+1}{2^N}\right). \tag{5}$$

Here, S is the number of sharable nodes, N is the number of layers and M is the number of theta cells involved. Thus, the total number of nodes Q for K egocentric place networks is

$$Q = M\left(1 - \frac{N+1}{2^N}\right) + KM\frac{N}{2^N} = M\left(1 + \frac{(K-1)N - 1}{2^N}\right). \tag{6}$$

The number of nodes or resources needed for multiple networks becomes less significant as the number of layers increases. In the current setup, we could use $20 + 4 \times 40 = 180$ nodes instead of $4 \times 60 = 240$ for the implemented basis, avert needing more DSP capacity than is provided by the SPARTAN-6 FPGA used here.

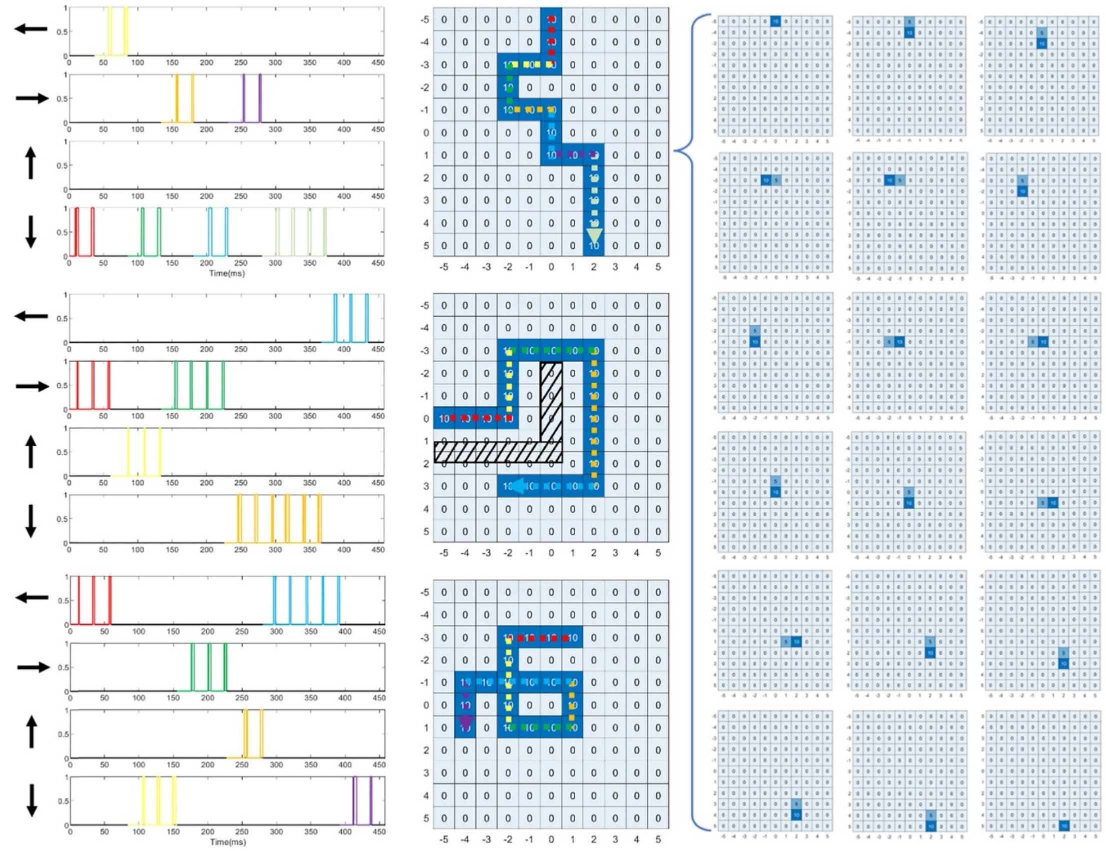

Figure 11. We simulated a grid of 11 × 11 place cells to validate its localization function. Three different paths are inputted to the theta chip in the form of velocity sequences. The first of these simulates the agent walking down the arena while looking around. The second simulates the agent circumventing an obstacle to reach its destination at [3, −2]. The third one simulates the agent walking a loop. The recorded traces of the four simultaneously operating egocentric place cells are shown on the left column with colored coded sections corresponding to the movement shown in the middle column. The panels in the middle column mark all the place cells that fired along the trail. The collection of panels on the right shows the place cells in action when receive a pulse from the egocentric place cells, along the first path. The activity bump marked by a value of 10 moves to the next place cell while leaving a trailing tail of 5 because of the global leakage of 5.

To conduct a tracking experiment, commands for controlling input velocity and resetting to the theta chip are issued from the host PC to the FPGA then relayed to the theta chip, then the PC records the output from the egocentric place cells and feeds the traces into the place cell network described in section 5. The Cap-clear signal is generated at the beginning of the trail and when any egocentric place cell fires, or a change in input velocity. Currently, for ease of display, the place cell network is simulated in MATLAB. It is trivial to implement the place cell network in its current state on a FPGA or a general-purpose neuromorphic chip given the modular design and simple logic. But we believe it can be further developed to perform mapping and navigation functionalities with the interconnection between place cells; this prospect will be explored in the discussion.

Three of the experiments in figure 11 demonstrate tracking capability with the implemented egocentric place cell networks receiving inputs from the theta chip. The travel is sequenced into segments as shown by the color code in figure 11. In the current experiments, each segment is encoded as a change of velocity command to load the theta chip's input DAC with the new velocity and held the Cap-clear signal high to commence a phase reset. The first path simulates the agent traveling along while randomly looking around. The second simulates the agent circumventing an obstacle to reach a certain destination, and the third tests the place cell network's ability to handle a trajectory with a loop. Each pulse from the egocentric place cells triggers the migration of the activity bump towards to the next respecting cell to track of the location. A phase reset procedure is conducted by the pulse of any egocentric place cell. If the robot travels along the same direction, multiple pulses are observed from the same egocentric place cells reporting multiple segments along that direction. The artifacts in the raw output from the egocentric place cells, as shown in figure 10, are filtered by the input port of the place cell layer thus will not cause errors in the next layer as discussed before. We use 5 as the step size for each place cell's activity level to allow clearer differentiation. A value of 10 means that a place cell is currently firing; 5 means that it was firing then decayed by a universal leak parameter of 5. We use this scheme to create a trailing tail for a better demonstration of the travel direction, shown in figure 11. We can see that the place cell network can successfully accumulate the egocentric place cell pulses to become a tracking map in an absolute spatial location given any path.

7. Discussion

We have demonstrated a neuromorphic structure for the formation of place cells with a simple digitized interference network that shows localization and path tracking capabilities in a place cell network. Our theta chip shows variations just like those that Welday *et al* observed in biological theta cells. We validated the robustness of the OI model proposed in [22] with our theta chip and FPGA implementation. We also designed a simple place cell network to convert the segmented displacement information of the OI model in [22] into a functional localization system.

The proven effectiveness of the improved OI model opens possibilities for neuromorphic implementations of a neuromorphic SLAM system. The model's tolerance towards theta cells allows for an analog implementation for lower layers. Our analog structure for the behavior model of theta cells serves as an example. Other theta cell implementations with more biologically plausible structures can also be developed through our structure without strict restrictions on accuracy or linearity. Moreover, with our network structure, variability of the analog circuits can be utilized to substitute the programmability requirement of the preferred velocity.

The theta chip can also be repurposed for any other models for place or grid cells since it encodes movements. Both OI model and CAN model require cells performing such task. Given the non-uniform nature due to its analog circuits, it provides a validation platform for the robustness of any neuromorphic or even neuroscience model. Furthermore, since mathematically the chip performs an approximation of vector projection operation, applications in other fields is also probable such as convolution or pattern recognition.

Our theta chip functions as a valid input layer despite the fact it operates at a much higher frequency range (∼2500 Hz) than is observed in biology (∼8 Hz). This issue shortens the phase-reset period, thus reducing the operation domain for the egocentric place cells. We will consider reducing the operating frequency of the theta chip in our next iteration.

The improved OI model provides a potential explanation of the functionality of grid cells for localization. The nodes in the second layer of our network structure can form grid cell behavior as shown in figure 1. Thus, grid cells not only participate in the localization, but also serve the purposes of variation reduction. In the second layer, there are two possibilities of pairing. The one implemented in this paper is that the pair is formed by nodes with the same orientation but opposite direction, resulting in a sparse stripe pattern as shown by the green arrow in figures 1(d) and (g). The other pairing strategy, shown in figure 1(i-iii), is the pair formed by lower-layer nodes with different orientations that could generate grid cell patterns such as the red arrow in the figure. Interestingly, both types of cells have been observed in biology [29]. Our model can serve as a guide for researching the properties of those cells in biology.

Furthermore, the basis formed by the egocentric place cells collectively forms a grid cell's response. For example, plotting the four signals together as one cell in a tracking trail in figure 11 shows how this cell is triggered in a square-grid fashion. A hexagonal grid can be implemented simply by replacing the current orthogonal basis with 6 basis vectors separated by 60°. Our model then provides an explanation of how grid cells tessellate. Interestingly, this explanation suggests that the grid cell's main function is to generate the phase reset signals for the theta cells.

We have hinted several times at the potential of the place cell network we proposed, especially the potential of the yet-to-exist direct connections between the place cells. Since the place cell network encodes the space in a coherent map, conventional path finding algorithms can be applied for a complete SLAM system. Any smart algorithm targeting at finding the optimized path requires some form of knowledge between the current location and the destination. We believe that the connection between place cells can broadcast distance information through the diffusion of the interconnections between place cells, given that the place cells can perform memory tasks. Then, a computed path can be expressed as a sequence of path cells by which to perform the navigation task. Furthermore, a more dynamic navigation algorithm can be combined with the flexible spatial encoding capability of the place cell network through connection with egocentric place cells with different magnitudes. These topics will be our group's future research toward a complete neuromorphic SLAM system.

In summary: we proposed and validated a neuromorphic system inspired by the hippocampus for spatial localization. The system can track the location of a moving agent under the influence of variations among the system with a simplified digital interference and still reproduce the behavior of place cells. Overall, the proposed system provides a concise and implementable platform for a more efficient neuromorphic SLAM system.

Appendix

Table A1. Characteristics of the theta chip.

Technology	TSMC 65 nm
Number of theta units	128
Maximum output phases	$1024 = 128^*8$
Die area	1.5 mm × 1 mm
Typical frequency range	1206–3066 Hz
Typical mean frequency (Mean/STD)	2023.771/374.611 Hz
Typical of gain coefficient (Mean/STD)	20.802/3.688 Hz per unit inner product
Digital power supply	3.3 V
Analog power supply	1 V
Maximum scanning clock	10 MHz
Typical scanning clock	6 MHz
Typical power consumption	6.2 mW
Output oscillation duty cycle	∼50%
Range of input/Preferred velocity [4-bit digital]	Range for better linearity [−4, 4], Max: [−7, 7]

DAC linearity	
Ideal range	0.2–0.3875 V
Ideal LSB	0.0125 V
Actual Range	0.2058–0.3824 V
DNL	0.224 LSB
INL	−0.872 LSB
Zero scale error	0.464 LSB
Offset error	5.8 mV
Gain error	−5.81%
Full scale error	−2.72%

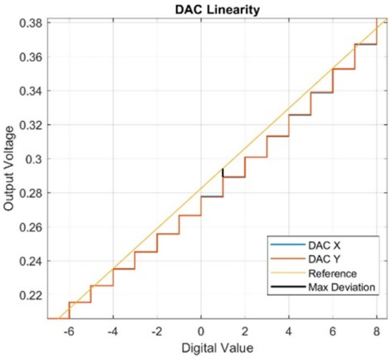

Data availability statement

The data cannot be made publicly available upon publication because they contain commercially sensitive information. The data that support the findings of this study are available upon reasonable request from the authors.

Acknowledgments

This work was partially funded via a Cooperative Agreement between JHU and Toshiba Corporation, NSF, and a Graduate Student Fellowship to Alia Nasrallah from the Government of Kuwait.

ORCID iD

Zhaoqi Chen https://orcid.org/0000-0003-2716-7495

References

[1] Khairuddin A R, Talib M S and Haron H 2015 Review on simultaneous localization and mapping (SLAM) *2015 IEEE Int. Conf. on Control System, Computing and Engineering (ICCSCE)*

[2] Milford M J, Wyeth G F and Prasser D 2004 RatSLAM: a hippocampal model for simultaneous localization and mapping *IEEE Int. Conf. on Robotics and Automation, 2004*

[3] Ball D, Heath S, Wiles J, Wyeth G, Corke P and Milford M 2013 OpenRatSLAM: an open source brain-based SLAM system *Auton. Robots* **34** 149–76

[4] Milford M, Jacobson A, Chen Z and Wyeth G 2016 RatSLAM: using models of rodent hippocampus for robot navigation and beyond *Robotics Research: The 16th Int. Symp. ISRR*

[5] Chen Z, Lowry S, Jacobson A, Hasselmo M E and Milford M 2015 Bio-inspired homogeneous multi-scale place recognition *Neural Netw.* **72** 48–61

[6] Milford M and Wyeth G 2010 Persistent navigation and mapping using a biologically inspired SLAM system *Int. J. Robot. Res.* **29** 1131–53

[7] O'Keefe J and Dostrovsky J 1971 The hippocampus as a spatial map: preliminary evidence from unit activity in the freely-moving rat *Brain Res.* **34** 171–5

[8] Hafting T, Fyhn M, Molden S, Moser M-B and Moser E I 2005 Microstructure of a spatial map in the entorhinal cortex *Nature* **436** 801–6

[9] O'keefe J and Burgess N 2005 Dual phase and rate coding in hippocampal place cells: theoretical significance and relationship to entorhinal grid cells *Hippocampus* **15** 853–66

[10] Moser E I, Kropff E and Moser M-B 2008 Place cells, grid cells, and the brain's spatial representation system *Annu. Rev. Neurosci.* **31** 69–89

[11] Sargolini F, Fyhn M, Hafting T, McNaughton B L, Witter M P, Moser M-B and Moser E I 2006 Conjunctive representation of position, direction, and velocity in entorhinal cortex *Science* **312** 758–62

[12] Indiveri G *et al* 2011 Neuromorphic silicon neuron circuits *Front. Neurosci.* **5** 73

[13] Samsonovich A and McNaughton B L 1997 Path integration and cognitive mapping in a continuous attractor neural network model *J. Neurosci.* **17** 5900–20

[14] Burak Y and Fiete I R 2009 Accurate path integration in continuous attractor network models of grid cells *PLoS Comput. Biol.* **5** e1000291

[15] Conklin J and Eliasmith C 2005 A controlled attractor network model of path integration in the rat *J. Comput. Neurosci.* **18** 183–203

[16] Burgess N, Barry C and O'keefe J 2007 An oscillatory interference model of grid cell firing *Hippocampus* **17** 801–12

[17] Burgess N 2008 Grid cells and theta as oscillatory interference: theory and predictions *Hippocampus* **18** 1157–74

[18] Hasselmo M E, Giocomo L M and Zilli E A 2007 Grid cell firing may arise from interference of theta frequency membrane potential oscillations in single neurons *Hippocampus* **17** 1252–71

[19] Welday A C, Shlifer I G, Bloom M L, Zhang K and Blair H T 2011 Cosine directional tuning of theta cell burst frequencies: evidence for spatial coding by oscillatory interference *J. Neurosci.* **31** 16157–76

[20] Cellon A B, Eisape A A, Furuta M and Etienne-Cummings R 2019 Velocity-controlled oscillators for hippocampal navigation on spiking neuromorphic hardware *2019 IEEE Int. Symp. on Circuits and Systems (ISCAS)*

[21] Nasrallah A, Chen Z, Alemohammad M, Balaji A, Cellon A, Furuta M and Etienne-Cummings R 2020 Velocity-tuned oscillators for NeuroSLAM and spatial navigation *2020 IEEE Int. Symp. on Circuits and Systems (ISCAS)*

[22] Zhaoqi C, Nasrallah A, Alemohammad M, Furuta M and Etienne-Cummings R 2022 Neuromorphic model of hippocampus place cells using an oscillatory interference technique for hardware implementation *Neuromorph. Comput. Eng.* **2** 044013

[23] Mhatre H, Gorchetchnikov A and Grossberg S 2012 Grid cell hexagonal patterns formed by fast self-organized learning within entorhinal cortex *Hippocampus* **22** 320–34

[24] Gupta S, Saxena V, Campbell K A and Baker R J 2009 W-2W current steering dac for programming phase change memory *2009 IEEE Workshop on Microelectronics and Electron Devices*

[25] Varghese V, Molin J L, Brandli C, Chen S and Cummings R E 2015 Dynamically reconfigurable silicon array of generalized integrate-and-fire neurons *2015 IEEE Biomedical Circuits and Systems Conf. (Biocas)*

[26] Folowosele F, Hamilton T J and Etienne-Cummings R 2011 Silicon modeling of the Mihalaş–Niebur neuron *IEEE Trans. Neural Netw.* **22** 1915–27

[27] Molin J L, Eisape A, Thakur C S, Varghese V, Brandli C and Etienne-Cummings R 2017 Low-power, low-mismatch, highly-dense array of VLSI Mihalas–Niebur neurons *2017 IEEE Int. Symp. on Circuits and Systems (ISCAS)*

[28] Kraetzschmar G K, Gassull G P and Uhl K 2004 Probabilistic quadtrees for variable-resolution mapping of large environments *IFAC Proc. Vol.* **37** 675–80

[29] Krupic J, Burgess N and O'Keefe J 2012 Neural representations of location composed of spatially periodic bands *Science* **337** 853–7